JACS
JOURNAL OF THE AMERICAN CHEMICAL SOCIETY

ARTICLE

pubs.acs.org/JACS

Total Synthesis of Pinnatoxins A and G and Revision of the Mode of Action of Pinnatoxin A

Romulo Araoz,[†] Denis Servent,[‡] Jordi Molgó,[†] Bogdan I. Iorga,[§] Carole Fruchart-Gaillard,[‡] Evelyne Benoit,[†] Zhenhua Gu,[⊥] Craig Stivala,[⊥] and Armen Zakarian*[,⊥]

[†]Institut de Neurobiologie Alfred Fessard, FRC2118, Laboratoire de Neurobiologie et Développement, UPR-3294, and [§]Institut de Chimie des Substances Naturelles, UPR 2301, Centre National de la Recherche Scientifique, F-91198 Gif-sur-Yvette cedex, France

[‡]Service d'Ingénierie Moléculaire des Protéines, Laboratoire de Toxinologie Moléculaire et Biotechnologies, Commissariat à l'Energie Atomique, F-91191 Gif-sur-Yvette, France

[⊥]Department of Chemistry and Biochemistry, University of California, Santa Barbara, California 93106-9510, United States

Supporting Information

ABSTRACT: Pinnatoxins belong to an emerging class of potent marine toxins of the cyclic imine group. Detailed studies of their biological effects have been impeded by unavailability of the complex natural product from natural sources. This work describes the development of a robust, scalable synthetic sequence relying on a convergent strategy that delivered a sufficient amount of the toxin for detailed biological studies and its commercialization for use by other research groups and regulatory agencies. A central transformation in the synthesis is the highly diastereoselective Ireland−Claisen rearrangement of a complex α,α-disubstituted allylic ester based on a unique mode for stereoselective enolization through a chirality match between the substrate and the lithium amide base. With synthetic pinnatoxin A, a detailed study has been performed that provides conclusive evidence for its mode of action as a potent inhibitor of nicotinic acetylcholine receptors selective for the human neuronal α7 subtype. The comprehensive electrophysiological, biochemical, and computational studies support the view that the spiroimine subunit of pinnatoxins is critical for blocking nicotinic acetylcholine receptor subtypes, as evidenced by analyzing the effect of a synthetic analogue of pinnatoxin A containing an open form of the imine ring. Our studies have paved the way for the production of certified standards to be used for mass-spectrometric determination of these toxins in marine matrices and for the development of tests to detect these toxins in contaminated shellfish.

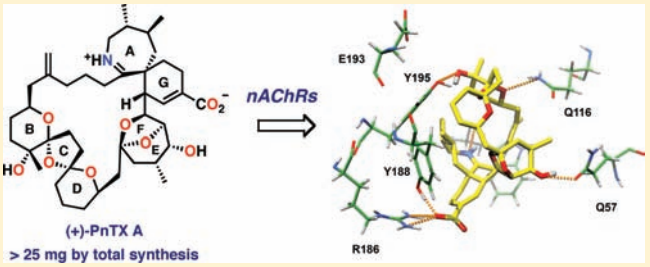

INTRODUCTION

Pinnatoxins are naturally occurring cyclic imines that comprise a newly emerging group of marine toxins with worldwide distribution.[1−3] Typically, marine toxins are classified and regulated on the basis of their toxicological profiles and mechanism of action; they can also be grouped on the basis of their chemical structures.[4] Many of the toxins have become indispensable reagents for fundamental research in biology. Regulatory control of marine algal toxins requires availability of pure, high-quality standards for toxicological and other relevant studies, as well as detailed information on the mechanism of biological activity. Previous studies with natural spirolides and gymnodimine—other members of the spiroimine group—revealed unique toxicological effects for this class of toxins in mice, where few symptoms are observed until a lethal dose is reached.[5,6] It is expected that a similar profile would be pronounced in humans, although no fatal cases involving the consumption of shellfish contaminated with cyclic imine toxins have been conclusively established thus far. Certified standards for pure spirolides and gymnodimine, but not for pinnatoxins, are available, although none of the spiroimine toxins are presently regulated.

Current data indicate that cyclic imine toxins are substantially less toxic by oral administration than by injection, with one probable exception being pinnatoxins.[7,8] Oral toxicity data are especially relevant for risk assessment of shellfish destined for human consumption. For pinnatoxins, extremely limited information is available due to their low and unreliable availability from natural sources, undermined by the fact that their producing organism has not been identified until recently in 2010.[7] Notwithstanding their highly intricate molecular structure, a chemical synthesis of pinnatoxins can provide an alternative source of high-quality material for biological and toxicological studies while also enabling fundamental studies aimed at a deeper understanding of their mode of action. It has been initially suggested that the mode of action of pinnatoxins involves calcium-channel activation.[9,10] However, there is a growing body

Received: February 9, 2011
Published: June 06, 2011

dx.doi.org/10.1021/ja201254c | J. Am. Chem. Soc. 2011, 133, 10499–10511

of evidence that a different mechanism of activity may be operational.[11]

The intricate molecular architecture of pinnatoxins creates abundant opportunities for innovation at the level of strategy, tactics, and invention of synthetic methods (Figure 1). Significant effort has been devoted to developing a chemical synthesis of pinnatoxins.[12−35] In 2008, we disclosed our original approach that resulted in completion of the total synthesis of (+)-pinnatoxin A.[32] In order for the methods and strategies developed for the synthesis of this complex structure to have a broader impact on biological and toxicological investigations, they must meet certain standards of efficiency and scalability. The previous synthetic endeavors that succeeded in reaching the natural product reported the production of only ∼1 mg quantities of pinnatoxins. In this article, we report the total synthesis of pinnatoxin A that has a capacity to satisfy the requirement of efficiency and scalability, furnishing substantial quantities of pinnatoxin A (PnTX A). With reliable access to synthetic PnTX A on scale, extensive electrophysiological, computational, and competition binding studies have been carried out that provide compelling evidence for its mode of action as an inhibitor of various subtypes of nicotinic acetylcholine receptors (nAChRs), redefining the originally proposed mechanism of bioactivity. In addition, we have found that PnTX A interacts selectively with the human neuronal α7 subtype of nicotinic receptors. We experimentally confirmed that the spiroimine fragment is the pharmacophore required for biological activity by examination of amino keto acid **2** (PnTX AK), which contains an open form of the imino ring A. The total synthesis of newly discovered pinnatoxin G, the putative biosynthetic progenitor for all pinnatoxins, is also reported. It has been proposed that the more toxic PnTX A is generated through metabolic oxidation of PnTX G after ingestion by shellfish.[8]

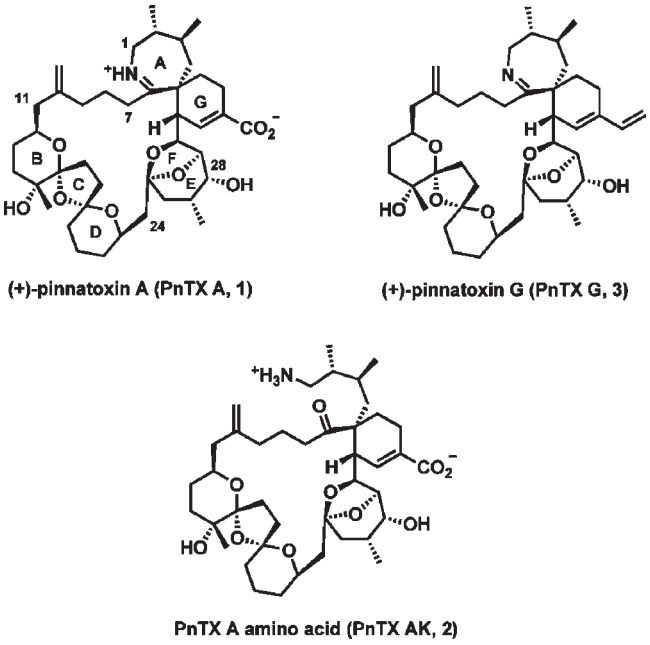

Figure 1. Natural pinnatoxins A and G and synthetic analogue PnTX AK with the acyclic amino ketone that are the subject of the synthetic and biological studies described in this article.

RESULTS AND DISCUSSION

Synthesis of (+)-Pinnatoxins A and G. *Synthesis Design.* The structure of pinnatoxin A is composed of the characteristic AG-spiroimine and BCD-dispiroketal domains connected by the C7−C11 acyclic carbon chain and the bridged EF-ketal, suggesting a convergent synthesis plan as outlined in Scheme 1. The general strategy was developed during the first-generation synthesis and is based on (1) the diastereoselective Ireland−Claisen rearrangement for the construction of the challenging quaternary stereogenic center at C5; (2) fragment union by a direct alkyllithium addition to aldehyde to form the C6−C7 bond; (3) the assembly of the 27-membered carbocycle by ring-closing metathesis introducing the C25−C26 double bond; and (4) EF-ketalization and installation of the imine ring (Scheme 1).[32] Several problematic transformations identified in the first-generation synthesis have been revised in order to enable the reproducible production of PnTX A on sufficient scale. The most important of these include modification of the substrate for ring-closing metathesis and the entire late-stage reaction sequence starting from compound **5** and culminating in the target molecule. The advanced 27-membered macrocyclic enone **5** was assembled by a convergent approach from two major building blocks, a G-ring aldehyde (**6**) and a BCD-bisketal fragment (**7**).

Synthesis of G-Ring Fragment. Synthesis of the G-ring aldehyde **6** incorporates another point of convergence beginning

Scheme 1. Overview of Synthesis Plan

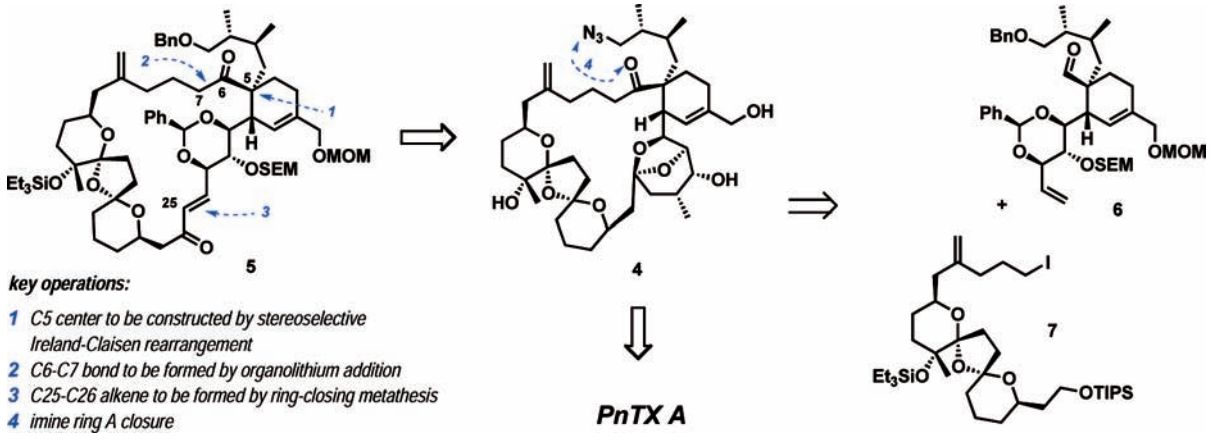

dx.doi.org/10.1021/ja201254c |J. Am. Chem. Soc. 2011, 133, 10499–10511

Scheme 2. Key Ireland−Claisen Rearrangement

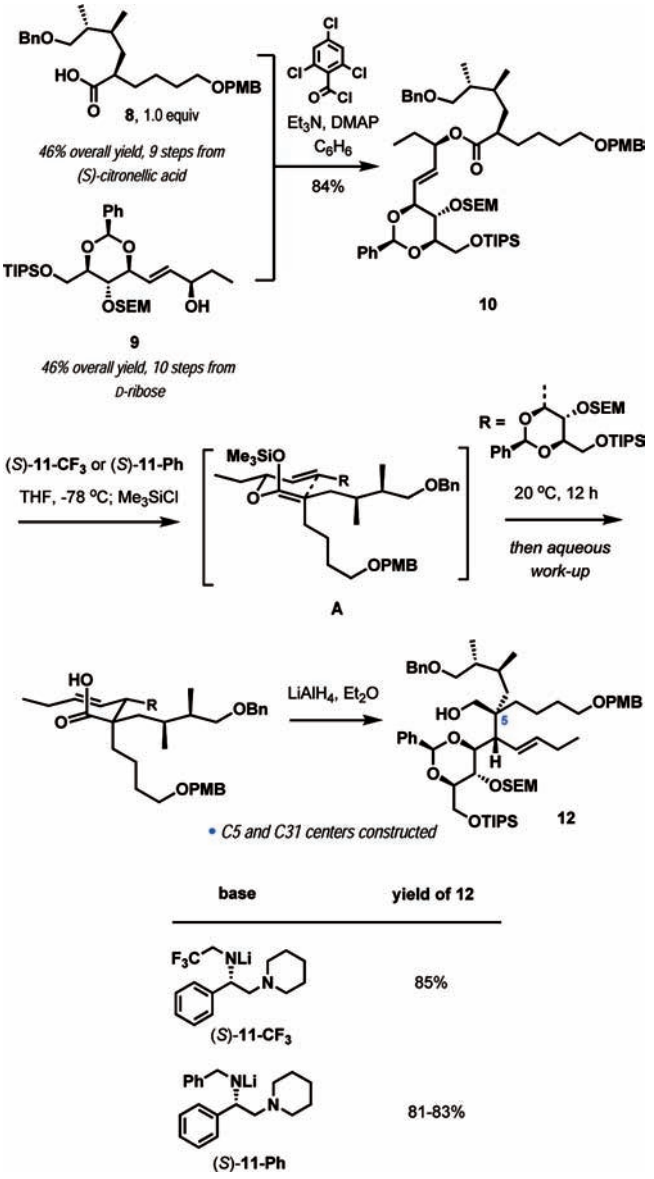

Scheme 3. Examples of Stereoselective Generation of Acyclic α,α-Disubstituted Enolates

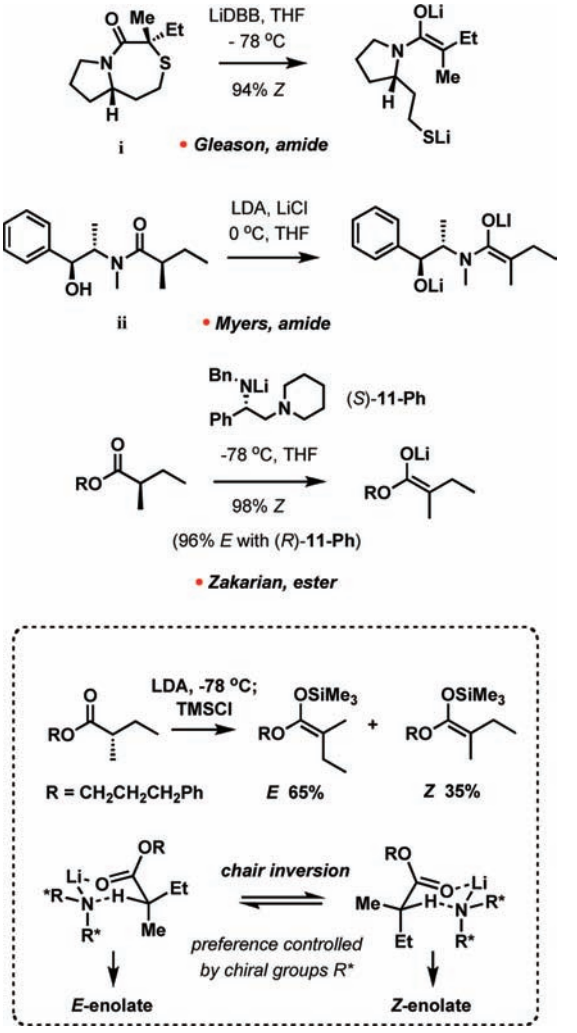

with a coupling of nearly equimolar amounts of carboxylic acid **8**[31] and allylic alcohol **9**, affording ester **10** in 84% yield (Scheme 2). We have found that the Yamaguchi protocol is superior to that employed originally [1.3 equiv of **8**, 1-ethyl-3-[3-(dimethylamino)propyl]carbodiimide (EDC), CH_2Cl_2, 94% yield based on **9**, 71% yield based on **8**] with equivalent amounts of **8** and **9**.[36]

A key operation in the synthesis is the installation of the quaternary stereogenic center at C5 (PnTX numbering), which was accomplished in the next step by a diastereoselective Ireland−Claisen rearrangement using a chiral lithium amide base. *N*-Trifluoroethyl-substituted lithium amide [(*S*)-**11**-CF_3] and benzyl-substituted lithium amide [(*S*)-**11**-Ph] gave comparable results with essentially complete stereocontrol in the formation of the *Z*-enolate (**A**).[37] After reduction of the intermediate carboxylic acid with $LiAlH_4$, the isolated yields of alcohol **12** were in the range of 81−85%. On scales in excess of 5 g of ester **10**, lithium amide (*S*)-**11**-Ph was preferred due to a lower cost associated with its large-scale production from inexpensive benzylamine. Each base can be recovered in high yield by a simple extraction with aqueous acid.

The efficient transfer of chirality in the rearrangement of ester **10** is enabled by a highly stereoselective enolization of the acyclic α,α-disubstituted ester affording a stereodefined tetrasubstituted enolate (**A**). The unusual mode of enolization, based on the chirality match between the ester and the reagent, was developed originally to address the problem of stereoselective installation of the C5 quaternary stereogenic center in the spiroimine toxins.[38] To date, this is the only general method for stereoselective generation of acyclic α,α-disubstituted ester enolates, although several methods for the synthesis of corresponding amide enolates have been developed recently (Scheme 3). Gleason and co-workers[39,40] pioneered a reductive enolization of thiazepinones such as **i** (Scheme 3) where the sense of stereoselectivity is determined by the ground-state conformation of the substrate. In 2008, Myers and co-workers[41] described the stereoselective generation of α,α-disubstituted enolates of amides **ii** (Scheme 3) derived from pseudoephedrine. The geometry of the enolate is, in part, an outcome of the relative configuration of the pseudoephedrine fragment and the α-position of the amide carbonyl

dx.doi.org/10.1021/ja201254c |*J. Am. Chem. Soc.* 2011, 133, 10499–10511

Scheme 4. Synthesis of G-Ring Aldehyde 6

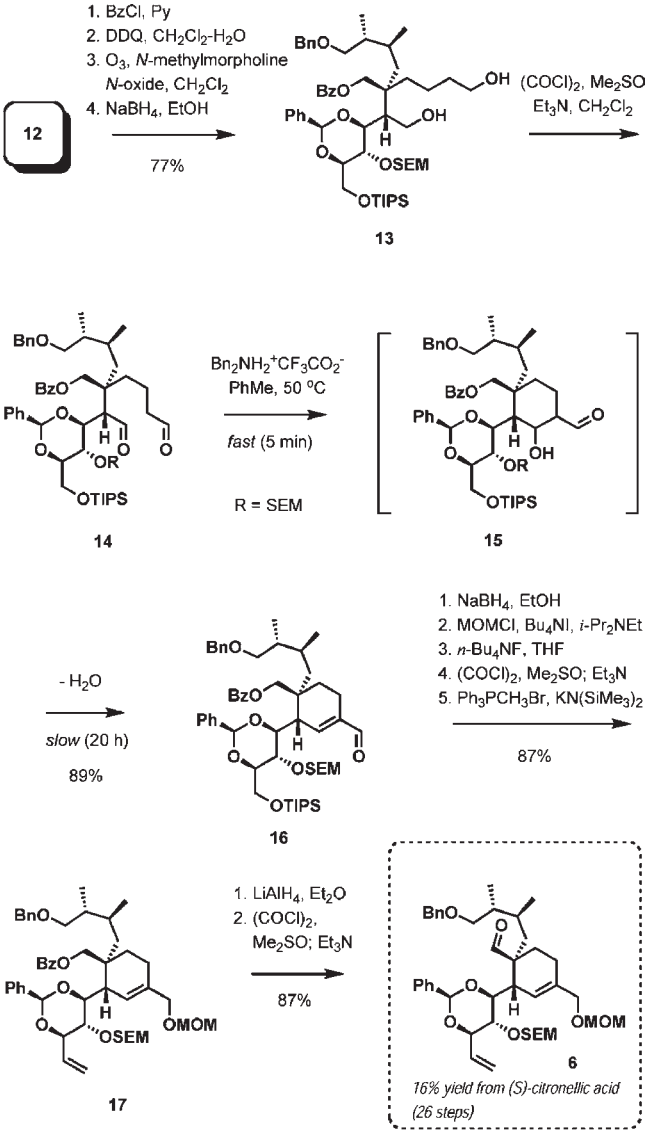

Scheme 5. Early Approach to BCD-Bisketal

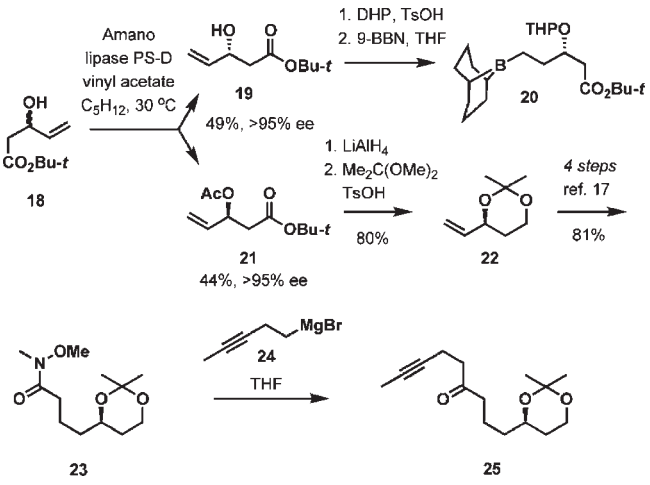

group. In the procedure developed in our laboratory, the configuration of the enolate is defined by the relative configuration of the ester and the chiral lithium amide. For example, enolization of 3-phenylpropyl (*S*)-2-methylbutyrate with (*S*)-**11**-Ph gives the *E*-enolate with 98% selectivity, whereas its enolization with the enantiomeric (*R*)-**11**-Ph produces the *Z*-enolate with 96% selectivity (Scheme 3).[38]

According to our hypothesis, the chiral base controls the conformational preference in the transition complex between the substrate and the reagent preceding the proton-transfer event. This conformational preference translates into the geometrical selectivity in enolate formation upon proton transfer. In Scheme 3, this concept is depicted by use of chairlike structures proposed by Ireland et al.,[42] although alternative conformationally defined transition structures are feasible, if not more plausible. Nonetheless, as long as the proton transfer occurs after precomplexation between the lithium amide and the ester, proceeding within a highly organized chiral system, the same logic will be applicable. There is strong evidence for precomplexation between lithium amide bases and carbonyl compounds prior to the proton transfer event in enolization reactions.[43−46]

With alcohol **12** in hand, diol **13** was secured in four additional steps that include benzoylation of the primary hydroxy group, oxidative removal of the *p*-methoxybenzyl protecting group, ozonolysis in the presence of *N*-methylmorpholine N-oxide according to the method of Dussault and co-workers,[47] and reduction with sodium borohydride (Scheme 4). The last reduction of the hydroxy aldehyde (not shown) to diol **13** was necessary because its direct oxidation to desired dialdehyde **14** was not successful with a variety of oxidants. A simultaneous oxidation of the two primary hydroxy groups in **13** to dialdehyde **14** was achieved under Swern conditions. Subsequent aldol cyclocondensation completed the formation of the G-ring. In this reaction, dibenzylammonium trifluoroacetate induced a cleaner transformation than piperidinium acetate, affording an 89% isolated yield of the desired product over two steps. The cyclocondensation was characterized by a rapid cyclization to aldol adduct **15**, which was followed by a slow dehydration to α,β-unsaturated aldehyde **16**.

The subsequent seven steps were necessary to prepare this fragment for coupling with BCD-precursor **7**. After reduction of the aldehyde, the allylic hydroxyl was protected as a methoxymethyl ether, the primary triisopropylsilyl (TIPS) ether was cleaved, and the resultant primary hydroxy group was oxidized to aldehyde, which was methylenated with the Wittig reagent to afford **17** in an 87% yield over five steps. Reductive removal of the benzoate followed by oxidation completed the synthesis of aldehyde **6** fully functionalized for fragment coupling in 16% overall yield, 26 linear steps from (*S*)-citronellic acid.

Synthesis of BCD-Bisketal Fragment. Synthesis of the BCD-bisketal fragment started with an efficient enzymatic resolution of *t*-butyl 3-hydroxy-4-pentenoate (Scheme 5).[17] Alcohol **19** was advanced to borane **20** in two steps, while acetate **21** was converted to Weinreb amide **23** via acetonide **22** in six steps following our original approach. During scaleup, we have found that the chain extension using 3-propyn-1-ylmagnesium bromide (**24**) was not reliable due to difficulties in efficient generation of the Grignard reagent. Various attempts to improve reproducibility of this transformation have not been productive, and as a recourse we opted for a direct installation of a more functionalized substituent incorporating a vinylsilane

Scheme 6. Assembly of BCD-Dispiroketal

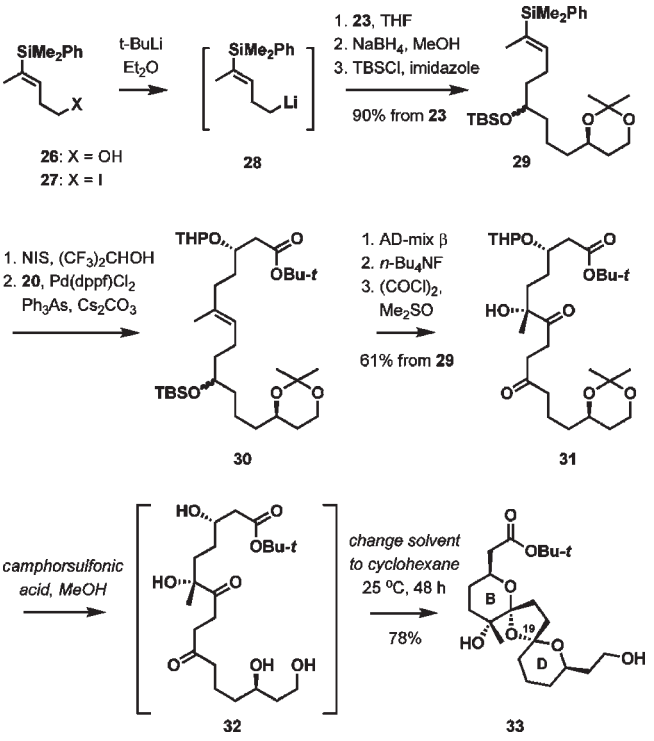

Table 1. Effect of Selective Silylation on Relative Stability of C19 Epimers

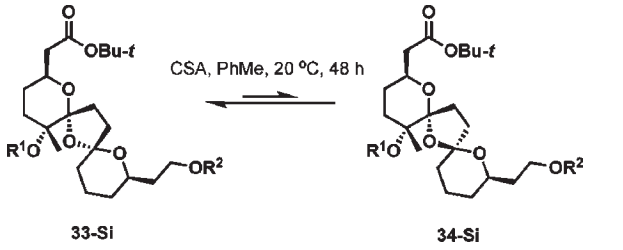

entry	R^1	R^2	33-Si:34-Si
1	H	H	4.0:1
2	H	*i*-Pr_3Si	1.7:1
3	Et_3Si	H	13:1
4	Et_3Si	*i*-Pr_3Si	8.3:1

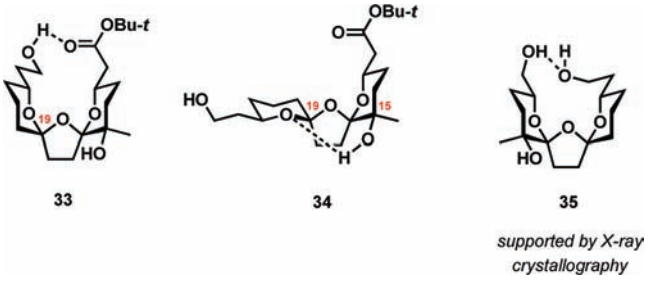

Figure 2. Hydrogen-bonding stabilization in spiroketal intermediates.

that served as a precursor to an iodoalkene required for further elaboration.

Iodide **27**, prepared from alcohol **26**, was subjected to lithium–iodine exchange that generated alkyllithium reagent **28**, which was coupled with amide **23** (Scheme 6). After two additional steps ($NaBH_4$, TBSCl), silane **29** was prepared in a scalable and reproducible manner. Stereoselective iododesilylation[48] and Suzuki–Miyaura coupling of the resultant iodoalkene with borane **20** in the presence of $Pd(dppf)Cl_2$ and Ph_3As afforded **30** in excellent yield.[49] Sharpless asymmetric dihydroxylation of the trisubstituted alkene,[50] desilylation, and double oxidation afforded diketone **31** in preparation for the BCD spirotricylic ketal formation. Removal of the acetal protecting groups ([tetrahydropyranyl (THP) and acetonide] upon exposure to acidic methanol at room temperature was accompanied by rapid ketalization of intermediate tetraol **32**. Upon extended reaction times, the desired diastereomer **33** is produced as a major product; however, the C19 epimer is formed initially and thus is favored under kinetic control.

A change of solvent from methanol to cyclohexane was performed to maximize diastereoselectivity in favor of **33** versus its C19 epimer. We initially ascribed the influence of the solvent on selectivity to the well-known enhancement of the anomeric effect in media of low polarity.[17] Upon superficial analysis, isomer **33** fully stabilized by anomeric effect should be increasingly more favored over its epimer **34** lacking anomeric stabilization at C19 as the medium polarity decreases, and indeed, this was consistent with our observations. Insightful contributions from the groups of Murai,[14,33,34] Hirama,[27,30] and Kishi[20] also suggest that the effect of intramolecular hydrogen-bonding stabilization should be considered. The C19 epimer **34** can be stabilized by a hydrogen bond between the tertiary hydroxy group at C15 and the D-ring oxygen, while the desired isomer is stabilized by long-range hydrogen bonding between the terminal ester and hydroxyl groups. The unusual long-range hydrogen bonding is supported by crystallographic studies reported by Hirama and coworkers[27] on enantiomeric bisketal **35** closely related to **33**. In order to further ascertain the effect of hydrogen bonding on the selectivity of spiroketalization, we carried out equilibration experiments with selectively silylated substrates. In all cases, the desired configuration at C19 was favored, but the level of preference varied substantially. As shown in Table 1, equilibration of the diol (entry 1) in the presence of camphorsulfonic acid in toluene at room temperature for 48 h resulted in a 4.0:1 mixture of diastereomers. The long-range H-bonding was disrupted by silylation of the primary hydroxy group (entry 2), which resulted in decrease in ratio to 1.7:1. Silylation of the tertiary hydroxyl group (Et_3Si) increased the ratio significantly to 13:1 (entry 3). When both hydroxyl groups were silylated, an 8.3:1 ratio of the isomers was recorded at equilibrium (entry 4). These results indicate that when only the anomeric effect is operational in the fully silylated substrate (entry 3), the thermodynamic ratio of 8.3:1 is observed in toluene, and hydrogen bonding from both tertiary and primary hydroxyl groups as depicted in Figure 2 has a significant effect on the position of the equilibrium.

In anticipation of the fragment coupling, the ester group in the fully silylated BCD-bisketal was reduced to aldehyde **36**. Addition of 3-(*p*-methoxybenzyloxy)-1-propyllithium followed by oxidation and methylenation afforded **37** in 76% yield over the previous seven steps (Scheme 7). We have found that the two-step Peterson olefination[51] procedure was substantially better suited for large-scale operations rather than the originally

dx.doi.org/10.1021/ja201254c |J. Am. Chem. Soc. 2011, 133, 10499–10511

Scheme 7. Completion of Synthesis of the BCD-Bisketal Fragment

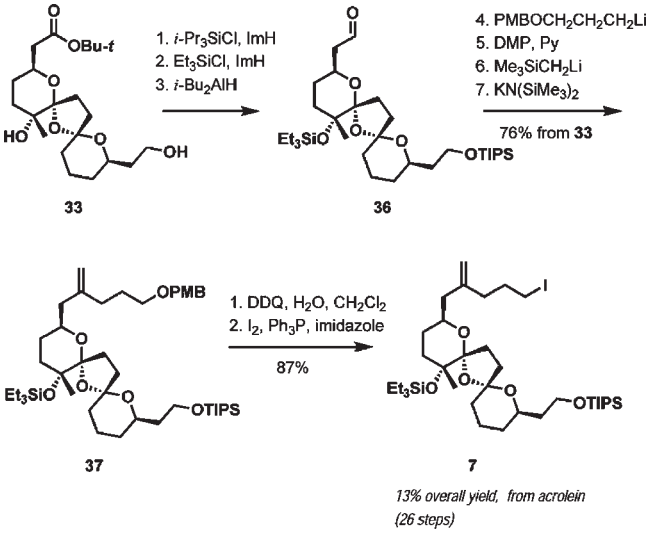

employed one-step Takai olefination.[52] The Wittig protocol was accompanied by ~30% epimerization at the C12 position. The synthesis of fully elaborated BCD-fragment **7** was completed in two additional steps, affording **7** in 13% overall yield over 26 steps from acrolein (Scheme 7).

Fragment Coupling and Completion of Total Synthesis. Unification of the two major fragments on a multigram scale was accomplished by direct addition of the complex organolithium reagent generated from **7** by lithium−iodine exchange to aldehyde **6**, with a 1:1 stoichiometry maintained for the two intermediates (78% yield). Unreacted aldehyde **6** was recovered in 16% yield. From **38**, the substrate for ring-closing metathesis was obtained in three steps involving selective desilylation, oxidation to ketoaldehyde, and chemoselective addition of vinylmagnesium bromide, giving a 1:1 mixture of diastereomeric alcohols **39** in 76% overall yield.

Preserving the silylation of the tertiary hydroxy group at C15 was essential for high regioselectivity in the ring-closing metathesis of **39**, a crucial transformation leading to the 27-membered carbocyclic framework of pinnatoxins. With catalyst **40** (20 mol %),[53] the ring closure was accomplished with >12:1 selectivity favoring 27-membered carbocycle **41** (75% isolated yield). The 17-membered macrocyclic byproduct **42** (6% isolated yield) was formed by ring-closing metathesis that engaged the methylene group at C10. The relative amount of the regioisomeric product was substantially larger with a free C15-hydroxy group. When the tertiary alcohol was desilylated, the ring-closing metathesis occurred with 3:1 regioselectivity under a variety of reaction conditions. The reasons for the change in selectivity are unclear but can possibly be understood as a result of subtle conformational differences between **39** and its desilylated analogue.

The final stereogenic center was established by oxidation of **41** to enone (85%) and conjugate addition of lithium methylcyanocuprate in the presence of boron trifluoride etherate (86%), which took place in an anti fashion relative to the C28 alkoxy substituent with high stereoselectivity.[54]

The objective of the next set of transformations was assembly of the macrocyclic framework of pinnatoxins through construction of the EF-ketal and introduction of a nitrogen substituent at the C1 position. Originally, EF-ketal formation was accomplished first. followed by debenzylation and azidation at C1. We discovered that the overall efficiency and scalability is substantially improved if the C1-azido group is introduced first. Two critical steps were facilitated by this reversal. First, open-chain EF-ketal precursor **43** is better suited for oxidative debenzylation because of its apparently higher resistance to oxidative decomposition in the presence of 2,3-dichloro-5,6-dicyanobenzoquinone (DDQ). Second, azide **44** proved to be a superior substrate for multiple deacetalization and EF-ketal formation under aqueous acidic conditions compared to its C1-benzyloxy analogue, delivering azido triol **4** in 71% yield in a reproducible fashion. The preparation of a total of 0.37 g (0.50 mmol) of **4** was enabled by this approach.

Synthetic (+)-PnTX A was obtained in six additional steps that began with oxidation of the allylic hydroxy group to carboxylic acid, followed by formation of the methyl ester. Although a free carboxyl group is present in the final compound, introduction of the methyl ester significantly improved the efficiency of material purification after reduction of the azide to primary amine, which was achieved by hydrogenation in the presence of Pd-$CaCO_3$. The imine formation was readily accomplished under modified Kishi conditions (triethylammonium mesitoate, PhMe, 85 °C, 60 h). Final hydrolysis of the methyl ester with lithium hydroxide in aqueous tetrahydrofuran (THF) delivered the natural product (Scheme 8). For the purposes of biological studies, 22 mg of the synthetic toxin has been prepared from 55 mg of **4**.

Synthesis of newly discovered pinnatoxin G (PnTX G) was completed by diverting some of the stock of azido triol **4** for this purpose (Scheme 9). The vinyl group was introduced in two steps by selective oxidation of the allylic hydroxy group to aldehyde [2,2,6,6-tetramethyl-1-piperidinyloxy (TEMPO), PhI-$(OAc)_2$] and Wittig olefination (76% overall yield). Staudinger reduction, imine ring closure, and purification by reverse-phase HPLC afforded pure PnTX G as its trifluoroacetate. NMR data of the synthetic material were consistent with those reported for natural PnTX G.[8,55]

In order to determine whether the imine ring is required for biological activity of PnTX A, an amino ketone analogue (PnTX AK) was prepared by modifying the final steps of the total synthesis (Scheme 10). Azido acid **46** was obtained in two steps from azido triol **4** and subjected to hydrogenation in the presence of the Lindlar catalyst. The requisite amino acid was isolated after purification by reverse-phase HPLC in 35% yield. During azide reduction studies, we have found that both hydrogenolysis and Staudinger reduction conditions led to the formation of variable amounts of dimeric urea **47**, presumably formed due to the presence of CO_2 dissolved in the reaction medium.

PnTX A Blocks Human α7 and α4β2, and *Torpedo* $\alpha1_2\beta\gamma\delta$ nAChRs in *Xenopus* Oocytes. With reliable access to synthetic PnTX A established, we carried out pharmacological investigations guided by the flaccid paralysis effect observed after injection of PnTX A in mice, suggesting its potential interaction with nAChRs. The hypothesis is supported by recent reports that other toxins in the cyclic imine family, gymnodimine A and 13-desmethylspirolide C, block nAChRs.[11,56] Initial experiments were performed in oocytes expressing either the human α7 or α4β2 nAChRs. A good expression of both nAChR subtypes was obtained 2−4 days after injection of the corresponding cDNA, as judged by the peak amplitude of currents elicited by ACh perfusion. Thus, in oocytes expressing the α7 nAChR, the perfusion of 350 μM ACh

Scheme 8. Completion of Synthesis of PnTX A

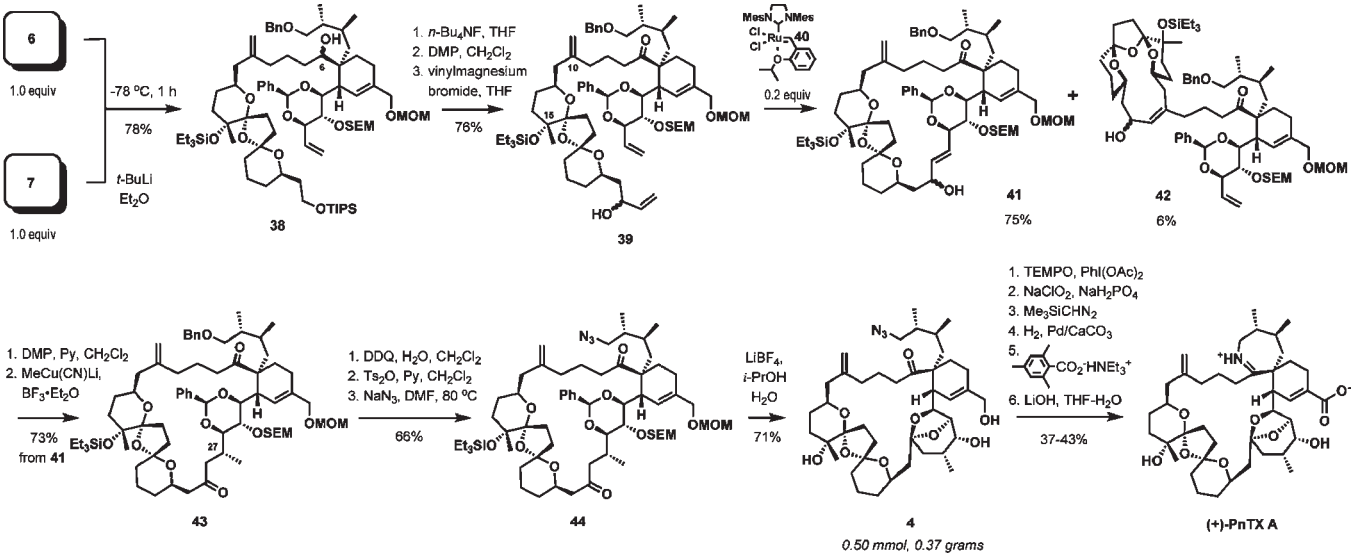

Scheme 9. Total Synthesis of PnTX G

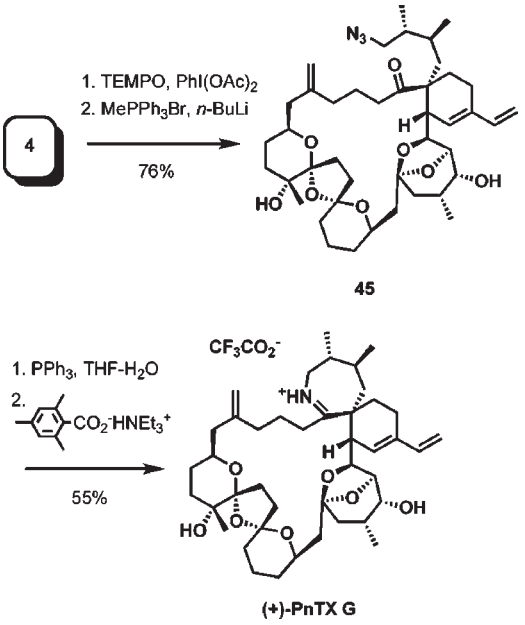

Scheme 10. Synthesis of Amino Ketone PnTX AK

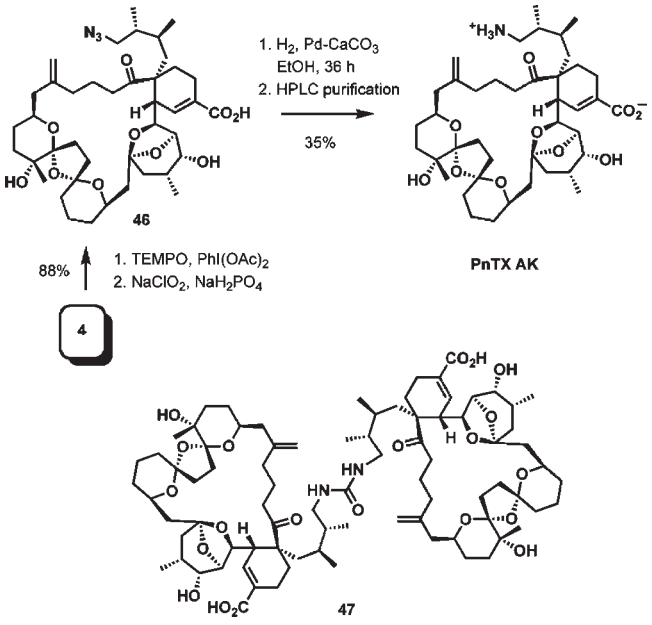

(corresponding to the EC_{50} determined experimentally) elicited peak currents that varied between oocytes and ranged from 1 to 3 μA at −60 mV holding membrane potential (n = 54 oocytes tested, from five donors). As shown in a typical recording (Figure 3A), the ACh-evoked currents started to desensitize within about 300 ms, but PnTX A did not appear to affect the rate of desensitization. In contrast, the ACh-evoked currents were markedly reduced in amplitude with pico- to nanomolar PnTX A concentrations, as shown in the concentration−inhibition curves (Figure 3D). PnTx G also blocked ACh-evoked currents in oocytes expressing the human α7 nAChR but was significantly less potent than PnTX A when their concentration−inhibition curves were compared [IC_{50} = 0.107 nM (0.086−0.132, 95% confidence interval) for PnTX A and 5.06 nM (3.84−6.67, 95% confidence interval) for PnTX G]. The blocking action of PnTX A on α7 nAChR was not reversible after a 10−15 min washout of the molecule from the medium. Furthermore, when applied on its own, PnTX A (0.1−50 nM) did not evoke any current, indicating that it has no direct agonist effect on the α7 nAChR subtype (n = 6). PnTX A also blocked the human α4β2 nAChR expressed in *Xenopus* oocytes, as shown in Figure 3C. However, higher PnTX A concentrations were needed to block the ACh-evoked currents (Table 2), indicating that the toxin was less potent in this neuronal receptor subtype, compared to the α7 nAChR (Figure 3D).

Microtransplantation of *Torpedo* nAChR into *Xenopus* oocytes has proven to be an elegant method to study its function and the

dx.doi.org/10.1021/ja201254c |J. Am. Chem. Soc. 2011, 133, 10499–10511

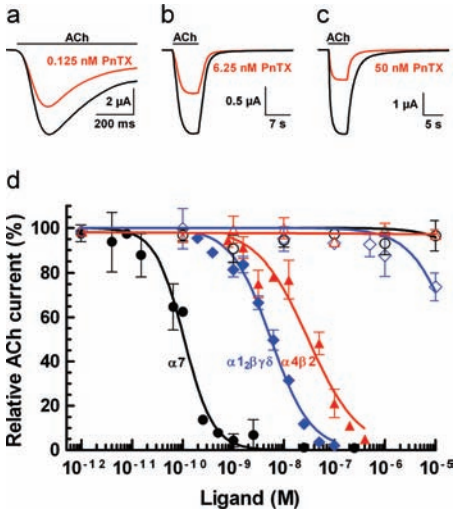

Figure 3. Effect of PnTX A and PnTX AK on nAChRs. ACh-evoked current was recorded at a holding potential of −60 mV in *Xenopus* oocytes expressing (a) human α7, (b) *Torpedo* $\alpha1_2\beta\gamma\delta$, and (c) human α4β2 nAChRs, before (black tracing) and after (red tracing) the action of PnTX A. The lines above current tracing indicate the time ACh was perfused. Note that PnTx A did not affect the rate of desensitization in the various nAChR subtypes. (d) Concentration-dependent inhibition of ACh-evoked currents by PnTX A or PnTX AK in *Xenopus* oocytes expressing the human α7 (solid circles, black curve) and α4β2 (solid triangles, red curve) neuronal nAChRs, or having incorporated into their membranes the *Torpedo* muscle type $\alpha1_2\beta\gamma\delta$ nAChR (solid diamonds, blue curve). Amplitudes of the ACh-current peak (mean ± SEM; 5 oocytes per concentration), recorded at a holding membrane potential of −60 mV, in the presence of either PnTX A or PnTX AK were normalized to control currents and fitted to the Hill equation (see Table 2 for IC_{50} values). Note the low activity of PnTX AK (open symbols; same colors apply for the curves as with PnTX A).

Table 2. Inhibition Constants for PnTX A on ACh-Evoked Nicotinic Currents in *Xenopus* Oocytes[a]

nAChR	PnTX A IC_{50}[b] (nM)
α7 (human)	0.107 (0.086−0.132)
α4β2 (human)	30.4 (19.4−47.5)
$\alpha1_2\beta\gamma\delta$ (*Torpedo*)	5.53 (4.5−6.8)

[a] Oocytes expressed human neuronal α7 or α4β2 nAChR subtypes or were microtransplanted with muscle-type $\alpha1_2\beta\gamma\delta$ nAChR. [b] Mean values from concentration−response curves were recorded on 46−50 oocytes for each experimental condition; 95% confidence intervals are shown in parentheses. For further details, see Figure 3.

effect of pharmacological agents.[57] Therefore, subsequent experiments were performed in oocytes with the *Torpedo* $\alpha1_2\beta\gamma\delta$ muscle-type nAChR incorporated into their membranes. PnTX A blocked the ACh-evoked nicotinic currents in muscle-type nAChR in a concentration-dependent manner (Figure 3D). Table 2 contains the IC_{50} data for PnTX A in both muscle- and neuronal-type nAChRs studied. An important finding is that the inhibitory potency of PnTX A is dependent on the nAChR receptor subtype. The order of potency established by the functional evaluation of PnTX A on nAChRs is α7 (human) > $\alpha1_2\beta\gamma\delta$ (*Torpedo*) > α4β2 (human), with IC_{50} values spanning 3 orders of magnitude from 0.1 to 30.4 nM (Table 2).

To determine whether the spiroimine fragment in PnTX A is required for the blocking action in nAChR subtypes, experiments

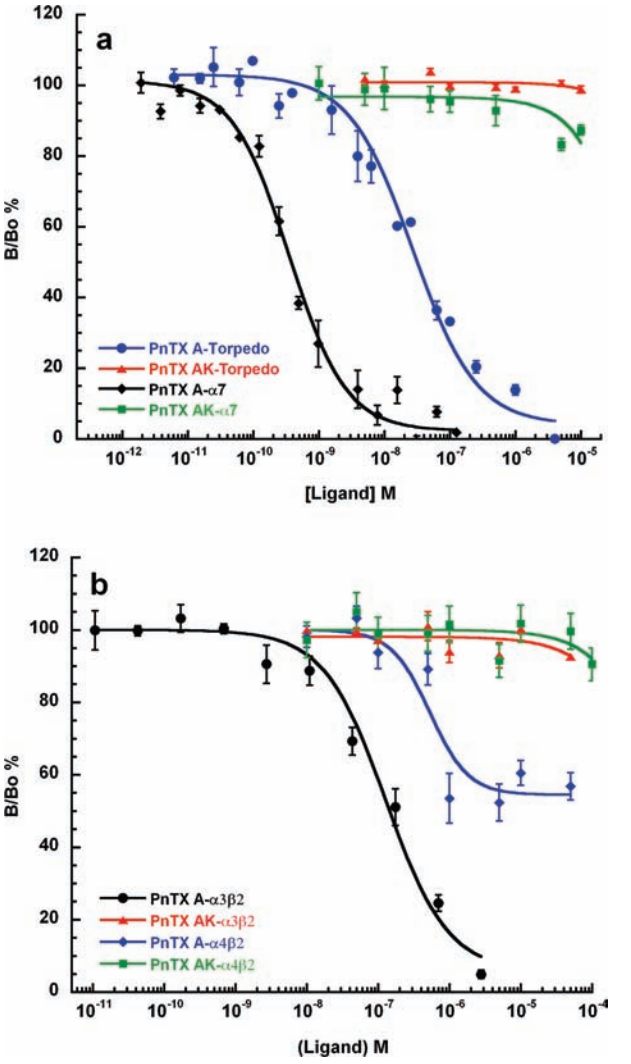

Figure 4. Effect of PnTX A and PnTX AK on various nAChRs. Inhibition of specific [^{125}I]α-BTX or (±)-[^{3}H]epibatidine binding by increasing concentrations of PnTX A or PnTX AK on (a) *Torpedo* and neuronal α7-5HT$_3$ or (b) heteropentameric α3β2 and α4β2 nAChRs. The results are expressed as the ratio of the specific radiotracer binding measured with (B) or without (B_0) competitive ligands, expressed as a percentage. Curve fitting was based on a nonlinear regression analysis using the Hill equation. Data are mean values ± SEM of at least three inhibition experiments.

were performed with PnTX AK amino keto acid (**2**), an analogue of PnTX A that contains an open form of the imine ring A. As shown in Figure 3D, PnTX AK had no action on the different nAChR subtypes expressed or incorporated into the membrane of *Xenopus* oocytes in the range of concentrations in which PnTX A blocked nAChRs. These results indicate that the spiroimine component is an important structural factor for blocking nAChRs by PnTX A.

Binding Competition Experiments between PnTX A and Radiolabeled Ligands. To get a deeper insight into the interaction between PnTX A and nAChR subtypes, competition binding studies were performed in HEK-293 cells expressing the chimeric chicken neuronal α7-5HT$_3$ and the human α4β2 and α3β2 nAChR subtypes and in *Torpedo* membranes expressing the muscle-type ($\alpha1_2\beta\gamma\delta$) nAChR, with both [^{125}I]α-bungarotoxin (α-BTX) and (±)-[^{3}H]epibatidine as radiotracers.

Table 3. Affinity Constants for PnTX A and Its Amino Keto Analogue (PnTX AK) on Muscle and Neuronal nAChR Subtypes[a]

	$K_i \pm$ SEM[b] (nM)			
ligand	$\alpha1_2\beta\gamma\delta$ (*Torpedo*)	$\alpha7-5HT_3$ (chick)	$\alpha4\beta2$ (human)	$\alpha3\beta2$ (human)
PnTX A	2.8 ± 0.03	0.35 ± 0.04	15.6 ± 5.2	9.4 ± 1.9
PnTX AK	>1000	>10 000	>2000	>2000

[a] Determined by equilibrium competition binding experiments. [b] Mean values ± SEM from three distinct experiments performed in duplicate.

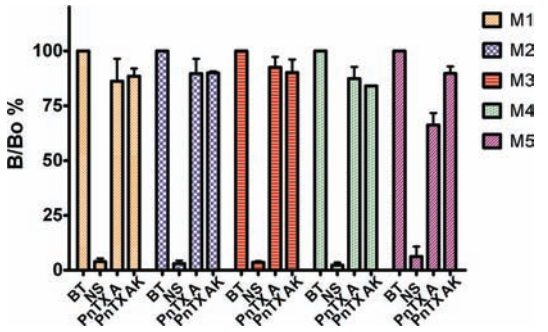

Figure 5. Inhibition of interaction of [^{3}H]NMS with five human mAChR subtypes by various ligands. The results for each receptor subtype are expressed as the ratio of the specific [^{3}H]NMS binding measured with (B) or without (B_0) the competitive ligands, expressed as a percentage. B_T is [^{3}H]NMS total binding, and NS is nonspecific binding in the presence of 50 μM atropine. Note that the effect of PnTX A and PnTX AK was evaluated at 1 μM concentration.

Competition binding curves obtained with PnTX A on muscle-type and homopentameric α7 neuronal receptors are shown in Figure 4A. These data tally well with competition for a single class of binding sites, and the apparent affinity constants (K_i) deduced from these experiments are reported in Table 3. PnTX A interacts with *Torpedo* and α7-5HT$_3$ receptors with high affinities respectively equal to 2.8 and 0.35 nM. Furthermore, PnTX A binds to the $\alpha3\beta2$ and $\alpha4\beta2$ heteropentameric neuronal receptors with affinities in the nanomolar range (Figure 4B, Table 3), and its order of potency on the various nAChRs subtypes is α7-5HT$_3$ > *Torpedo* > $\alpha3\beta2$ = $\alpha4\beta2$, confirming the results obtained with electrophysiological experiments. Interestingly, PnTX A displaces approximately half the [^{3}H]epibatidine in the $\alpha4\beta2$ receptor, revealing a partial antagonist property on this receptor subtype. Studies on the binding potency of PnTX AK on the muscle and neuronal nAChRs subtypes showed that this toxin produces no significant displacement of the radioactive tracer, even at high concentrations (Figure 4A,B), suggesting a decrease of at least 3 orders of magnitude in affinity as compared to PnTX A. Thus, disruption of the imine ring in PnTX A is responsible for the drastic loss of affinity of this compound for the various nAChR subtypes.

While the ability of cyclic imines to affect drastically the nicotinic function has now been clearly demonstrated, their action on other cholinergic neurotransmission pathways remained elusive due to the lack of purified PnTX A. With the ready access to pure PnTX A established in this study, the potential inhibitory activity of 1 μM PnTX A or PnTX AK was evaluated on CHO cells stably expressing the distinct human muscarinic acetylcholine receptor (mAChR) subtypes. As shown in Figure 5, both PnTX A and PnTx AK had no significant effect on ^{3}H-NMS binding to M1, M2, M3, and M4 mAChR subtypes, whereas PnTX A (1 μM) induced 35% radiotracer displacement in M5 mAChR (Figure 5), indicating a low micromolar affinity for this receptor subtype. Here again, this property was lost for the PnTX AK analogue that contains an open form of the imine ring A (**2**).

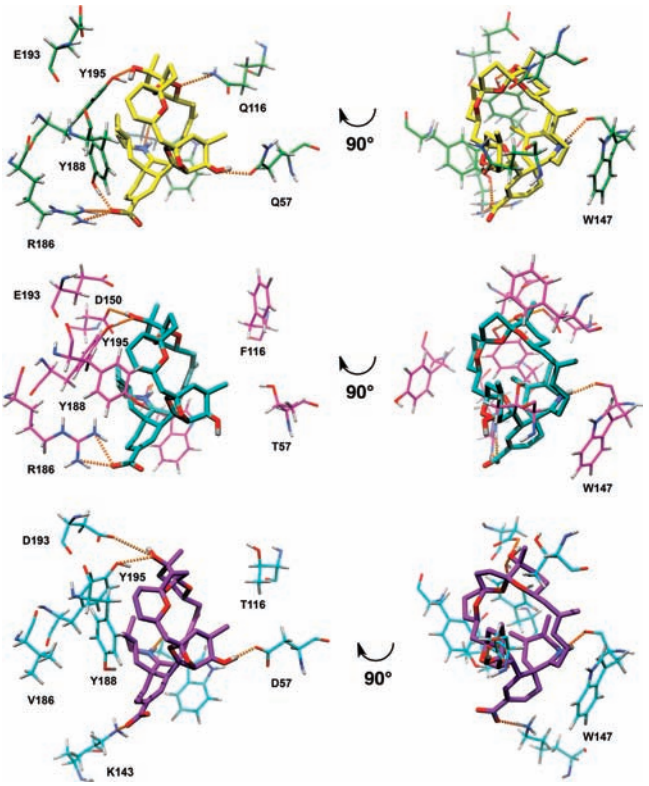

Figure 6. Representative protein−ligand interactions in PnTX A−nAChR complexes obtained by molecular modeling: (a) human α7 (green, α7−α7 interface), (b) human $\alpha4\beta2$ (magenta, α4−β2 interface), and (c) *Torpedo* $\alpha1\beta1\gamma\delta$ (cyan, α1−δ interface). Only amino acids interacting through hydrogen bonds with the ligand and the residues from equivalent positions in the sequence alignment are shown (see Supporting Information, Table 2-1, for further information). PnTX A is colored in (a) yellow, (b) light blue, and (c) violet, respectively. For each complex, two different views, rotated by 90°, are presented. Nonpolar hydrogen atoms of the ligand are not shown for clarity.

Computational Modeling of the PnTX A-nAChR interactions. Structural modeling of the PnTX A-nAChRs complexes revealed that the toxin is embedded within loops C and F of the receptor, involving mainly aromatic side chains of the principal and complementary faces (see Supporting Information for more details on molecular modeling protocols). The main protein−ligand interactions are shown in Figure 6, and a detailed analysis of residues surrounding PnTX A in the binding site is provided in Supporting Information, Table 2-1. The ligand is positioned in a similar manner in all three complexes, with differences in binding affinity arising mainly from the residue variability in key positions of the binding site. PnTX A establishes an important number of hydrogen bonds (seven) with α7 nAChR, which are well distributed in the binding site and involve most of the ligand's

functional groups. Conversely, only five hydrogen bonds are observed in the $\alpha4\beta2$ complex, covering approximately 50% of the binding site at a close distance. The $\alpha1_2\beta1\gamma\delta$ complex shows intermediate behavior, with the five hydrogen bonds more equally distributed in the binding site. The latter complex also benefits from important hydrophobic contacts with the complementary δ subunit; these interactions are substantially reduced in the $\alpha4\beta2$ complex. Most of the residues present in the binding site are conserved among the three nAChRs subtypes considered (residues 93, 143, 147, 149, 188, 190, 191, and 195 from the principal side and residues 55, 79, and 118 from the complementary side, highlighted in Supporting Information, Table 2-1), while in a few positions with amino acid variability the neighboring residues are able to compensate for the missing interaction (e.g., in $\alpha1_2\beta1\gamma\delta$, the carboxylate group of PnTX A is not able to establish an ionic interaction with Val186 as it does with the equivalent residue Arg186 in $\alpha7$ and $\alpha4\beta2$ nAChR subtypes; instead, it interacts with Lys143). However, in some cases, differences in amino acid sequence are responsible for changes in the protein−ligand interaction pattern. One example is Gln116 from the $\alpha7$ subtype, which interacts with an oxygen atom from the bis-spiroketal core, while the equivalent residues Phe116 from $\alpha4\beta2$ and Leu116 from the $\alpha1_2\beta1\gamma\delta$ subtype are unable to establish similar interactions. Similarly, Gln57 from the $\alpha7$ subtype and Asp57 from the $\alpha1_2\beta1\gamma\delta$ subtype form hydrogen bonds with a hydroxy group at the C28 position of PnTX A near the solvent-exposed site, whereas the side chain of the equivalent Thr57 residue from the $\alpha4\beta2$ subtype is too short to form analogous interactions. Overall, the protein−ligand interactions identified in these three complexes are in very good agreement with the experimentally determined biological properties, with PnTX A showing notably stronger interactions with the $\alpha7$ nAChR subtype compared to the $\alpha4\beta2$ subtype, while the $\alpha1_2\beta1\gamma\delta$ subtype displayed intermediate binding potency with significant hydrophobic contribution from the complementary side.

Pinnatoxin A: Selective Inhibition of nAChRs. The production of several milligrams of PnTX A enabled us to perform the first broad receptor binding screening and comprehensive functional and pharmacological characterization of this natural cyclic imine toxin with nicotinic acetylcholine receptors.[58] Indeed, until now, the mode of action of pinnatoxins was ascribed to action on calcium channels.[9] However, in our studies, even at 10 μM PnTX A, no significant binding activity was detected for calcium channels.[58] The symptoms observed upon intraperitoneal injection of a lethal dose of PnTX A in mice give a toxicological profile characterized by transient mouse hyperactivity, followed by a decrease in respiratory rate with prominent abdominal breathing leading to death due to respiratory paralysis. Such a toxicological profile is also seen with agents affecting nicotinic receptors in the central nervous system and in the skeletal neuromuscular junction. Furthermore, there is growing evidence that other structurally related cyclic imine toxins affect both muscle- and neuronal-type nAChRs.[11,56] The electrophysiological and binding studies described herein demonstrate the ability of PnTX A to interact very efficiently with various nAChR subtypes. The selectivity profile and affinity values determined by the two approaches were similar: $\alpha7$ (0.1−0.3 nM) > *Torpedo* (3−5 nM) > $\alpha3\beta2$ = $\alpha4\beta2$ (10−30 nM), demonstrating the ability of this toxin to recognize muscle as well as neuronal subtypes that potentially is at the origin of the toxicity of this compound. Furthermore, the apparent irreversibility of the PnTX A−nAChR interaction may reinforce its toxicological effect.

To determine whether the spiroimine fragment in PnTX A is required for its potent blockage of nAChR subtypes, experiments were performed with the PnTX AK analogue, which contains an acyclic form of the imine ring A. Both electrophysiological and binding assays showed the inactivity of PnTX AK with different nAChRs, highlighting the crucial role of the cyclic imine for the biological activity of PnTX A. This inactivity can be explained by the existence of conformers strongly stabilized by an intramolecular ionic interaction between the ammonium and carboxylate groups of PnTX AK in solution (see Supporting Information, Figure 2-2). These conformations, which are unable to bind directly to the nAChR subunit interface, would require an energetically unfavorable disruption of the intramolecular ion pair to produce an "open" form of the ligand, which could potentially interact with the binding site. These observations reinforce the functional role of the cyclic imine and the importance of its structural integrity for the interaction with nAChRs. The cyclic imine moiety represents the key feature in this family of toxins and its role in PnTX A binding to nAChRs, according to the modeling, is dual. First, in conjunction with the C28 hydroxy group of the bridged EF-ketal, it anchors the ligand to the binding site through hydrogen bonds in a conformation ideally positioned to optimize the interactions with neighboring residues. Moreover, the hydrogen bond established by this group with the backbone carbonyl of Trp147 is observed not only in all three docking complexes obtained in this work but also in the two crystal structures of the complexes between ACh binding protein (AChBP) and gymnodimine A or 13-desmethyl spirolide C.[11] Second, binding of the closed imino ring A in PnTX A appears to be more favorable, both sterically and energetically, than that of the corresponding open amino ketone form in PnTX AK. The presence of a protonated nitrogen could serve as a common functional signature in the cyclic imine phycotoxins, interacting with nicotinic receptors as has been shown for PnTX A (this work), gymnodimine A, and 13-desmethyl spirolide C[11,56] and that has yet to be demonstrated for pteriatoxins and prorocentrolides.

Finally, aside from their clear effect on nAChRs, interaction of cyclic imine toxins such as 13-desmethyl spirolide C with other targets of the cholinergic neurotransmission pathway, especially the muscarinic receptors (mAChRs), has also been reported recently.[59] Therefore, interaction of PnTX A and PnTX AK with the five human mAChR subtypes has been further evaluated at 1 μM concentration. Although no interaction was observed with M1, M2, M3, and M4 mAChR subtypes, a weak effect of PnTX A was measured for the M5 subtype, suggesting a low micromolar affinity of this toxin for the M5 receptor subtype. This weak interaction with the M5 receptor is at least 3 orders of magnitude lower compared to the interaction of PnTX A with various nAChRs and seems unlikely to be correlated with its toxicological profile.

■ CONCLUSION

The comprehensive study described here encompasses the scalable synthesis and thorough biological evaluation of PnTX A to conclusively establish its mechanism of toxicity as primarily due to its potent and effectively irreversible inhibition of nicotinic acetylcholine receptors. With respect to total synthesis, reliable access to PnTX A and PnTX G on scale was enabled by the development of new enolization technique based on a chiral

match between the ester substrate and the base. This allowed for a reliable control of stereoselectivity in the installation of the spiroimine fragment of the marine toxins. Late-stage operations including ring-closing metathesis, EF-ketal formation, and closure of the imine ring were developed and optimized, resulting in a relatively high overall yield of the natural products. Thus, PnTX A was accessed in a 1.4% overall yield, which is a several-fold improvement compared to previously described syntheses. By use of the chemistry developed in this synthesis effort, an analogue with an open imine ring, amino ketone PnTX AK, was prepared to determine the significance of the AG-spiroimine subunit as a pharmacophore. Subsequent comprehensive electrophysiological and competition binding studies confirmed the hypothesis that the spiroimine component of pinnatoxins is an important structural factor for blocking nAChRs. Furthermore, computational modeling studies provided further insight into the functional determinants and binding regions for both PnTX A and nAChR subtypes that are important for strong molecular interactions. Finally, chemical synthesis of the pinnatoxins and knowledge of their mode of action on nicotinic acetylcholine receptors pave the way for the production of certified standards to be used for mass spectrometry determination of toxins in marine matrices and for the development of tests to detect these toxins in contaminated shellfish.

EXPERIMENTAL SECTION

Pinnatoxins A, G, and AK and Radioligands. PnTX A, PnTX G, and the ketamine analogue (PnTX AK) were prepared by total synthesis as described herein. Detailed procedures and spectral data are presented in Supporting Information. Samples of synthetic PnTX A, PnTX G and PnTX AK were dissolved in ethanol and diluted in physiological solutions. The total ethanol concentration in the test solution did not exceed 0.15%. All physical data for synthetic PnTX A, PnTX AK, and PnTX G, including ^{1}H and ^{13}C NMR spectroscopy, high-resolution mass spectrometry (HRMS), HPLC, and optical rotation data showed both compounds to be of high purity and identical to natural samples. [^{125}I]α-Bungarotoxin ([^{125}I]α-BTX) (210−250 Ci·mmol^{-1}), (±)-[^{3}H]epibatidine (55 Ci·mmol^{-1}), and *N*-methyl-[^{3}H]scopolamine methyl chloride ([^{3}H]NMS) (78 Ci·mmol^{-1}) were purchased from Perkin-Elmer (Courtaboeuf, France). All other chemicals were obtained from Sigma−Aldrich (Saint Quentin Fallavier, France) or other usual sources.

Animals and Biological Materials. Adult female *Xenopus laevis* frogs were obtained from the Centre de Ressources Biologiques Xénope, CNRS (Université de Rennes 1, France). Live *Torpedo marmorata* fishes were purchased from the Service Modèles Biologiques of the Station Biologique de Roscoff (France). Live animals were maintained in the Animal Campus facility of Gif-sur-Yvette. Experiments were performed in accordance with European Community guidelines for laboratory animal handling and with the official edict presented by the French Ministry of Agriculture and the recommendations of the Helsinski Declaration. The cDNAs coding for chick chimeric α7-5HT$_3$, human α4β2,and human α3β2 were kindly provided by Dr. P. J. Corringer (Pasteur Institute, Paris, France) and by Professor O. Steinlein (Institute of Human Genetics, Bonn, Germany). The human α7 cDNA[60] was a generous gift from Professor I. Bermudez (Oxford Brookes University, Oxford, U.K.). Chinese hamster ovary (CHO) cells stably expressing the M1−M5 cloned human muscarinic acetylcholine receptors (mAChRs) were kindly provided by Professor P. O. Couraud (Institut Cochin de Génétique Moléculaire, Paris, France).

Expression of nAChRs in Human Embryonic Kidney (HEK-293) Cells. A chimeric cDNA of the neuronal type α7-5HT$_3$ nAChR was transfected into HEK-293 cells by calcium phosphate precipitation, as previously described.[56,61] Briefly, the chick cDNA (15 μg of α7-5HT$_3$) was transfected by calcium precipitation with careful control of the pH (6.95). The cells were placed at 37 °C under 5% CO_2, and 2 days after transfection, cells were harvested in phosphate-buffered saline (PBS) with 5 mM ethylenediaminetetraacetic acid (EDTA) and resuspended in 3 mL/plate of this buffer for binding experiments. For human α3β2 or α4β2 nAChR subtypes, 24 h after the calcium phosphate transfection (7 μg of α3 or α4, and 7 μg of β2) the cells were placed for 2 days at 30 °C, 5% CO_2 before being collected for binding assays, which used a cell density adjusted to specifically bind ≤10% of radioligand.

CHO Cells Expressing Human M1−M5 mAChRs and Membrane Preparation. CHO cells stably expressing M1−M5 mAChRs were grown in plastic Petri dishes (Falcon) and incubated at 37 °C in an atmosphere of 5% CO_2 and 95% humidified air in Ham F12 medium precomplemented with L-glutamine and bicarbonate and supplemented with 10% fetal calf serum and 1% penicillin/streptomycin. At 100% confluence, the medium was removed and cells were harvested in Versen buffer (PBS + 5 mM EDTA). They were washed with ice-cold phosphate buffer and centrifuged at 1700*g* for 10 min (4 °C). The pellet was suspended in ice-cold buffer (1 mM EDTA, 25 mM sodium phosphate, and 5 mM $MgCl_2$, pH 7.4) and homogenized with a Potter−Elvehjem homogenizer (Fisher Scientific Labosi, Elancourt, France). The homogenate was centrifuged at 1700*g* for 15 min (4 °C). The sediment was resuspended in buffer, homogenized, and centrifuged at 1700 g for 15 min (4 °C). The combined supernatants were centrifuged at 35000*g* for 30 min (4 °C) and the pellet was suspended in the same buffer (0.1 mL/dish). Protein concentrations were determined according to the Lowry method with bovine serum albumin (BSA) as standard. The membrane preparations were aliquotted and stored at −80 °C.

Binding Assays. The affinity of PnTX A and AK for the chimeric α7-5HT$_3$ nAChR was determined as previously described.[61,62] Briefly, cells expressing the α7-5HT$_3$ receptors were preincubated with different PnTX A concentrations and filtered through GF/C filters 6 min after the addition of 1 nM [^{125}I] α-BTX. The filters were washed with cold PBS and counted on a γ counter (LKB-Multigamma 1261, Uppsala, Sweden). The protection constant (K_p) calculated by fitting the competition data by the empirical Hill equation was shown to correspond to the dissociation constants.[63] Competition experiments with *Torpedo* nAChRs were performed at equilibrium by incubating (for at least 4 h) 0.05 μg of *Torpedo* membrane with different concentrations of PnTX A and [^{125}I]α-BTX (0.25−0.35 nM). The mixture was filtered, rinsed, and counted as previously described for the chimeric α7-5HT$_3$ nAChR. Equilibrium binding experiments on α4β2 and α3β2 subtypes used [^{3}H]epibatidine as radioactive tracer. Cells expressing these receptor subtypes were incubated with 0.5−1 nM [^{3}H]epibatidine and various concentrations of PnTX for 4 h. After filtration, GF/C filters were dried and 6 mL of scintillation solution (Ultima Gold F, PerkinElmer, France) was added before the filters were counted on a Liquid Scintillation Analyzers (Tri-Carb 2300 TR, Perkin-Elmer, France).

In equilibrium competition experiments, IC_{50} values were determined by fitting the competition data by the empirical Hill equation and converted to K_i constants via the equation $K_i = IC_{50}/(1 + L^*/K_d)$,[64] with K_d for α-BTX on muscle-type receptor of 50 pM and K_d for epibatidine on human α3β2 and α4β2 equal to 35 and 20 pM, respectively. All experiments were done at least three times in duplicate.

The effect of PnTX on the equilibrium binding of [^{3}H]NMS on the five mAChRs subtypes (M1−M5) was determined in inhibition experiments on 96-well plates. With [^{3}H]NMS as tracer, membrane protein concentrations was adjusted so that no more than 10% of added radioligand was specifically bound (around 1500−2500 cpm), and the plate was incubated in PBS−BSA at 25 °C for 120 min with micromolar concentrations of ligands and [^{3}H]NMS (0.5 nM), in a final assay volume of 100 μL. Nonspecific binding was determined in the presence of 50 μM atropine. The reaction was stopped by filtration of the 96-well plate simultaneously through a GF/C plate presoaked in 0.5% poly(ethylenimine), by use of a FilterMate harvester (Perkin-Elmer, France). The filters were washed twice with ice-cold buffer (PBS) and dried, and the bound radioactivity was counted, after the addition of 25 μL of MicroScint/well, by scintillation spectrometry on a TopCount β counter (PerkinElmer, France). Each experiment was done at least two times in duplicate.

Expression of Human α7 nAChR in *Xenopus* Oocytes. Oocytes were surgically removed from mature female *Xenopus laevis* frogs under anesthesia with ethyl-3-aminobenzoate methanesulfonate salt (Sigma−Aldrich, Saint Quentin Fallavier, France) solution (1.5 g/L), were treated for 10 min with 1 mg·mL^{-1} collagenase type I (Sigma−Aldrich) in calcium-free medium containing (in millimolar units) NaCl 88, KCl 2.5, $MgCl_2$ 1, and *N*-(2-hydroxyethyl)piperidine-*N*′-2-ethanesulfonic acis (HEPES) 5 (pH 7.6), and were manually defolliculated. Following an extensive washing with this solution, oocytes were transferred to Barth's solution containing (in millimolar units) NaCl 88, KCl 1, $MgSO_4$ 0.33, $CaCl_2$ 0.41, $MgSO_4$ 0.82, $Ca(NO_3)_2$ 0.33, $NaHCO_3$ 2.4, and HEPES 10 (pH 7.2) supplemented with streptomycin sulfate and 0.01 mg·mL^{-1} penicillin G. Oocytes were maintained at 19 °C for up to 4 days in this solution. Stage V−VI oocytes were selected and microinjected with 50 nL of human α7 cDNA (1 μg·μL^{-1}) or α4β2, as reported previously, by use of a Nanoliter 2000 Micro 4 Controller (World Precision Instruments, Inc., U.K.) mounted on a microscope. Recordings were performed 3−4 days after injection.

***Torpedo* Membrane Preparation and nAChR Microtransplantation to Oocytes.** *Torpedo marmorata* specimens kept in conventional artificial seawater were anesthetized with tricaine (Sigma−Aldrich), at a concentration of 0.03% in seawater, before surgical excision of electric organs. The $\alpha1_2\beta\gamma\delta$ nAChR-rich membranes were prepared at 4 °C from freshly dissected and sliced *Torpedo* electric organs by procedures previously described,[65] resuspended in 5 mM glycine, and stored aliquotted at −80 °C until use. Microtransplantation of *Torpedo* nAChR used microinjection into the oocyte cytoplasm of a membrane suspension (50 nL at 3.5 mg/mL protein) from a Nanoliter2000 Micro4 controller mounted on a microscope.

Voltage-Clamp Recording on Oocytes. ACh-evoked currents were recorded with a standard two-microelectrode voltage-clamp amplifier (OC-725B, Warner Instrument Corp., Hamden, CT) at a holding potential of −60 mV. Voltage and current microelectrodes were pulled from borosilicate glass to reach 0.5−1.5 MΩ tip resistance when filled with 3 M KCl. Data were acquired with a pCLAMP-9/Digidata-1322A system (Molecular Devices, Union City, CA). The recording chamber (capacity 300 μL) was superfused (8−12 mL/min; 20 °C) with a modified Ringer's solution containing (in millimolar units) NaCl 100, KCl 2.8, $BaCl_2$ 0.3, and HEPES 5 (pH 7.4), where $BaCl_2$ substitution for $CaCl_2$ prevents secondary activation of a Ca^{2+}-dependent Cl^- current.[66] Oocytes were initially incubated for 3 min with the respective PnTX A or its amino keto analogue and then ACh was applied, for 3 s in oocytes expressing the human α7 nAChR or for 15 s for human α4β2 as well as for the *Torpedo* ($\alpha1_2\beta\gamma\delta$) nAChR incorporated to the oocyte membrane, by use of a computer-controlled solution exchange system (VC-6; Warner Instruments). Between successive ACh applications, 4-min perfusion intervals with modified Ringer's were maintained to ensure receptor recovery from desensitization.

Concentration−Inhibition Analysis of ACh Currents. Dose−response curves for agonist activation were analyzed by using the equation $I = I_{max}[L]^n/(EC_{50} + [L])^{n_H}$, where I is the measured agonist-evoked current, [L] is the agonist concentration, EC_{50} is the agonist concentration that evoked half the maximal current (I_{max}), and n_H is the Hill coefficient. I values were normalized to the I_{max} value recorded from the same oocyte, to yield fractional (percent) response data. The IC_{50} was determined from dose−response curves by fitting to the equation $F = 1/[1 + ([X]/IC_{50})^{n_H}]$, where F is the fractional response obtained in the presence of the inhibitor at concentration [X] and IC_{50} is the inhibitor concentration that reduced the ACh-evoked amplitude by half.

■ ASSOCIATED CONTENT

Supporting Information. (1) Full experimental procedures for the synthesis of pinnatoxins A and G; (2) text, two figures, and one table with details of computational molecular modeling; (3) ^{1}H and ^{13}C NMR and HPLC spectra; and (4) one table and one figure showing binding assay data. This material is available free of charge via the Internet at http://pubs.acs.org.

■ AUTHOR INFORMATION

Corresponding Author
zakarian@chem.ucsb.edu

■ ACKNOWLEDGMENT

Receptor binding data for over 40 receptors, transporters, and ion channels were generously provided by the National Institute of Mental Health's Psychoactive Drug Screening Program, Contract HHSN-271-2008-025C (NIMH PDSP). The NIMH PDSP is directed by Bryan L. Roth. M.D., Ph.D., at the University of North Carolina at Chapel Hill and Project Officer Jamie Driscol at NIMH, Bethesda, MD. We thank Dr. Jon Evans (UNC Chapel Hill) for assistance. This research was supported by the U.S. National Institutes of Health (NIGMS, GM077379 to A.Z. with subcontract KK1036 to J.M.) and by the CNRS and the CEA. We are grateful to P. Villeneuve and G. Esnault (CNRS) and E. Bindundu (CEA) for technical assistance. C.S. is supported by Tobacco-Related Disease Research Program Dissertation Award and the UCSB Dean's Fellowship. Eli Lilly and Amgen provided additional unrestricted support (A.Z.).

REFERENCES

(1) Cembella, A.; Krock, B. In *Seafood and Freshwater Toxins*, 2nd ed.; Botana, L. M., Ed.; CRC Press: Boca Raton, FL, 2008; pp 561−580.
(2) Gueret, S. M.; Brimble, M. A. *Nat. Prod. Rep.* **2010**, *27*, 1350–1366.
(3) Munday, R. In *Seafood and Freshwater Toxins*, 2nd ed.; Botana, L. M., Ed.; CRC Press: Boca Raton, FL, 2008; pp 581−594.
(4) Aune, T. In *Seafood and Freshwater Toxins*, 2nd ed.; Botana, L. M., Ed.; CRC Press: Boca Raton, FL, 2008; pp 3−20.
(5) Hu, T.; Burton, I. W.; Cembella, A. D.; Curtis, J. M.; Quilliam, M. A.; Walter, J. A.; Wright, J. L. C. *J. Nat. Prod.* **2001**, *64*, 308–312.
(6) Munday, R.; Towers, N. R.; Mackenzie, L.; Beuzenberg, V.; Holland, P. T.; Miles, C. O. *Toxicon* **2004**, *44*, 173–178.
(7) Rhodes, L.; Smith, K.; Selwood, A. I.; McNabb, P.; van Ginkel, R.; Holland, P. T.; Munday, R. *Harmful Algae* **2010**, *9*, 384–389.
(8) Selwood, A. I.; Miles, C. O.; Wilkins, A. L.; van, G. R.; Munday, R.; Rise, F.; McNabb, P. *J. Agric. Food Chem.* **2010**, *58*, 6532–6542.
(9) Zheng, S.; Huang, F.; Chen, S.; Tan, X.; Zuo, J.; Peng, J.; Xie, R. *Zhongguo Haiyang Yaowu* **1990**, *9*, 33–35.
(10) Uemura, D.; Chou, T.; Haino, T.; Nagatsu, A.; Fukuzawa, S.; Zheng, S.-z.; Chen, H.-s. *J. Am. Chem. Soc.* **1995**, *117*, 1155–1156.
(11) Bourne, Y.; Radic, Z.; Araoz, R.; Talley, T. T.; Benoit, E.; Servent, D.; Taylor, P.; Molgó, J.; Marchot, P. *Proc. Natl. Acad. Sci. U.S.A.* **2010**, *107*, 6076–6081.
(12) Hao, J.; Matsuura, F.; Kishi, Y.; Kita, M.; Uemura, D.; Asai, N.; Iwashita, T. *J. Am. Chem. Soc.* **2006**, *128*, 7742–7743.
(13) Ishihara, J.; Horie, M.; Shimada, Y.; Tojo, S.; Murai, A. *Synlett* **2002**, 403–406.
(14) Ishihara, J.; Sugimoto, T.; Murai, A. *Synlett* **1998**, 603–606.
(15) Ishihara, J.; Tojo, S.; Kamikawa, A.; Murai, A. *Chem. Commun.* **2001**, 1392–1393.
(16) Ishiwata, A.; Sakamoto, S.; Noda, T.; Hirama, M. *Synlett* **1999**, 692–694.
(17) Lu, C.-D.; Zakarian, A. *Org. Lett.* **2007**, *9*, 3161–3163.
(18) Matsuura, F.; Hao, J.; Reents, R.; Kishi, Y. *Org. Lett.* **2006**, *8*, 3327–3330.
(19) Matsuura, F.; Peters, R.; Anada, M.; Harried, S. S.; Hao, J.; Kishi, Y. *J. Am. Chem. Soc.* **2006**, *128*, 7463–7465.
(20) McCauley, J. A.; Nagasawa, K.; Lander, P. A.; Mischke, S. G.; Semones, M. A.; Kishi, Y. *J. Am. Chem. Soc.* **1998**, *120*, 7647–7648.
(21) Nakamura, S.; Inagaki, J.; Kudo, M.; Sugimoto, T.; Obara, K.; Nakajima, M.; Hashimoto, S. *Tetrahedron* **2002**, *58*, 10353–10374.
(22) Nakamura, S.; Inagaki, J.; Sugimoto, T.; Kudo, M.; Nakajima, M.; Hashimoto, S. *Org. Lett.* **2001**, *3*, 4075–4078.
(23) Nakamura, S.; Inagaki, J.; Sugimoto, T.; Ura, Y.; Hashimoto, S. *Tetrahedron* **2002**, *58*, 10375–10386.
(24) Nakamura, S.; Kikuchi, F.; Hashimoto, S. *Tetrahedron: Asymmetry* **2008**, *19*, 1059–1067.
(25) Nakamura, S.; Kikuchi, F.; Hashimoto, S. *Angew. Chem., Int. Ed.* **2008**, *47*, 7091–7094.
(26) Nitta, A.; Ishiwata, A.; Noda, T.; Hirama, M. *Synlett* **1999**, 695–696.
(27) Noda, T.; Ishiwata, A.; Uemura, S.; Sakamoto, S.; Hirama, M. *Synlett* **1998**, 298–300.
(28) Pelc, M. J.; Zakarian, A. *Org. Lett.* **2005**, *7*, 1629–1631.
(29) Pelc, M. J.; Zakarian, A. *Tetrahedron Lett.* **2006**, *47*, 7519–7523.
(30) Sakamoto, S.; Sakazaki, H.; Hagiwara, K.; Kamada, K.; Ishii, K.; Noda, T.; Inoue, M.; Hirama, M. *Angew. Chem., Int. Ed.* **2004**, *43*, 6505–6510.
(31) Stivala, C. E.; Zakarian, A. *Tetrahedron Lett.* **2007**, *48*, 6845–6848.
(32) Stivala, C. E.; Zakarian, A. *J. Am. Chem. Soc.* **2008**, *130*, 3774–3776.
(33) Sugimoto, T.; Ishihara, J.; Murai, A. *Tetrahedron Lett.* **1997**, *38*, 7379–7382.
(34) Sugimoto, T.; Ishihara, J.; Murai, A. *Synlett* **1999**, 541–544.
(35) Suthers, B. D.; Jacobs, M. F.; Kitching, W. *Tetrahedron Lett.* **1998**, *39*, 2621–2624.
(36) Inanaga, J.; Hirata, K.; Saeki, H.; Katsuki, T.; Yamaguchi, M. *Bull. Chem. Soc. Jpn.* **1979**, *52*, 1989–1993.
(37) Gu, Z.; Herrmann, A. T.; Stivala, C. E.; Zakarian, A. *Synlett* **2010**, 1717–1722.
(38) Qin, Y.-c.; Stivala, C. E.; Zakarian, A. *Angew. Chem., Int. Ed.* **2007**, *46*, 7466–7469.
(39) Manthorpe, J. M.; Gleason, J. L. *J. Am. Chem. Soc.* **2001**, *123*, 2091–2092.
(40) Tiong, E. A.; Gleason, J. L. *Org. Lett.* **2009**, *11*, 1725–1728.
(41) Kummer, D. A.; Chain, W. J.; Morales, M. R.; Quiroga, O.; Myers, A. G. *J. Am. Chem. Soc.* **2008**, *130*, 13231–13233.
(42) Ireland, R. E.; Mueller, R. H.; Willard, A. K. *J. Am. Chem. Soc.* **1976**, *98*, 2868–2877.
(43) Ramirez, A.; Sun, X.; Collum, D. B. *J. Am. Chem. Soc.* **2006**, *128*, 10326–10336.
(44) Sun, X.; Collum, D. B. *J. Am. Chem. Soc.* **2000**, *122*, 2452–2458.
(45) Sun, X.; Collum, D. B. *J. Am. Chem. Soc.* **2000**, *122*, 2459–2463.
(46) Sun, X.; Kenkre, S. L.; Remenar, J. F.; Gilchrist, J. H.; Collum, D. B. *J. Am. Chem. Soc.* **1997**, *119*, 4765–4766.
(47) Schwartz, C.; Raible, J.; Mott, K.; Dussault, P. H. *Org. Lett.* **2006**, *8*, 3199–3201.
(48) Ilardi, E. A.; Stivala, C. E.; Zakarian, A. *Org. Lett.* **2008**, *10*, 1727–1730.
(49) Miyaura, N.; Suzuki, A. *Chem. Rev.* **1995**, *95*, 2457–2483.
(50) Kolb, H. C.; VanNieuwenhze, M. S.; Sharpless, K. B. *Chem. Rev.* **1994**, *94*, 2483–2547.
(51) Peterson, D. J. *J. Org. Chem.* **1968**, *33*, 780–784.
(52) Takai, K.; Nitta, K.; Utimoto, K. *J. Am. Chem. Soc.* **1986**, *108*, 7408–7410.
(53) Garber, S. B.; Kingsbury, J. S.; Gray, B. L.; Hoveyda, A. H. *J. Am. Chem. Soc.* **2000**, *122*, 8168–8179.
(54) Yamamoto, Y.; Chounan, Y.; Nishii, S.; Ibuka, T.; Kitahara, H. *J. Am. Chem. Soc.* **1992**, *114*, 7652–7660.
(55) Kuduk, S. D.; DiPardo, R. M.; Chang, R. K.; Ng, C.; Bock, M. G. *Tetrahedron Lett.* **2004**, *45*, 6641.
(56) Kharrat, R.; Servent, D.; Girard, E.; Ouanounou, G.; Amar, M.; Marrouchi, R.; Benoit, E.; Molgó, J. *J. Neurochem.* **2008**, *107*, 952–963.
(57) Eusebi, F.; Palma, E.; Amici, M.; Miledi, R. *Progress in Neurobiology* **2009**, *88*, 32–40.
(58) Receptor binding data for over 40 receptors, transporters, and ion channels were generously provided by the National Institute of Mental Health's Psychoactive Drug Screening Program (see Acknowledgment). See Supporting Information 4 for additional details.
(59) Wandscheer, C. B.; Vilarino, N.; Espina, B.; Louzao, M. C.; Botana, L. M. *Chem. Res. Toxicol.* **2010**, *23*, 1753–1761.
(60) Maskell, P. D.; Speder, P.; Newberry, N. R.; Bermudez, I. *Br. J. Pharmacol.* **2003**, *140*, 1313–1319.
(61) Servent, D.; Winckler-Dietrich, V.; Hu, H.-Y.; Kessler, P.; Drevet, P.; Bertrand, D.; Ménez, A. *J. Biol. Chem.* **1997**, *272*, 24279–24286.
(62) Eisele, J.-L.; Bertrand, S.; Galzi, J.-L.; Devillers-Thiery, A.; Changeux, J.-P.; Bertrand, D. *Nature* **1993**, *366*, 479–483.
(63) Weber, M.; Changeux, J.-P. *Mol. Pharmacol.* **1974**, *10*, 1–14.
(64) Cheng, Y..; Prusoff, W. H. *Biochem. Pharmacol.* **1973**, *22*, 3099–3108.
(65) Krieger, F.; Mourot, A.; Araoz, R.; Kotzyba-Hibert, F.; Molgó, J.; Bamberg, E.; Goeldner, M. *ChemBioChem* **2008**, *9*, 1146–1153.
(66) Sands, S. B.; Costa, A. C.; Patrick, J. W. *Biophys. J.* **1993**, *65*, 2614–2621.